Clinical Cancer Research

# *In Vivo* Hemin Conditioning Targets the Vascular and Immunologic Compartments and Restrains Prostate Tumor Development

Felipe M. Jaworski[1,2,3], Lucas D. Gentilini[2,3], Geraldine Gueron[1,3], Roberto P. Meiss[4], Emiliano G. Ortiz[1,3], Paula M. Berguer[5], Asif Ahmed[6], Nora Navone[7], Gabriel A. Rabinovich[8,9], Daniel Compagno[2,3], Diego J. Laderach[2,3,10], and Elba S. Vazquez[1,3]

## Abstract

**Purpose:** Conditioning strategies constitute a relatively unexplored and exciting opportunity to shape tumor fate by targeting the tumor microenvironment. In this study, we assessed how hemin, a pharmacologic inducer of heme oxygenase-1 (HO-1), has an impact on prostate cancer development in an *in vivo* conditioning model.

**Experimental Design:** The stroma of C57BL/6 mice was conditioned by subcutaneous administration of hemin prior to TRAMP-C1 tumor challenge. Complementary *in vitro* and *in vivo* assays were performed to evaluate hemin effect on both angiogenesis and the immune response. To gain clinical insight, we used prostate cancer patient-derived samples in our studies to assess the expression of HO-1 and other relevant genes.

**Results:** Conditioning resulted in increased tumor latency and decreased initial growth rate. Histologic analysis of tumors grown in conditioned mice revealed impaired vascularization. Hemin-treated human umbilical vein endothelial cells (HUVEC) exhibited decreased tubulogenesis *in vitro* only in the presence of TRAMP-C1–conditioned media. Subcutaneous hemin conditioning hindered tumor-associated neovascularization in an *in vivo* Matrigel plug assay. In addition, hemin boosted $CD8^+$ T-cell proliferation and degranulation *in vitro* and antigen-specific cytotoxicity *in vivo*. A significant systemic increase in $CD8^+$ T-cell frequency was observed in preconditioned tumor-bearing mice. Tumors from hemin-conditioned mice showed reduced expression of galectin-1 (Gal-1), key modulator of tumor angiogenesis and immunity, evidencing persistent remodeling of the microenvironment. We also found a subset of prostate cancer patient-derived xenografts and prostate cancer patient samples with mild HO-1 and low Gal-1 expression levels.

**Conclusions:** These results highlight a novel function of a human-used drug as a means of boosting the antitumor response. *Clin Cancer Res; 23(17); 5135–48. ©2017 AACR.*



## Introduction

Prostate cancer is the second most common cancer in men worldwide (1). Although most current therapies against this disease are designed to target the tumor cells, the surrounding microenvironment plays a leading role in enabling tumor development (2). Novel cancer therapies should consider the crosstalk between epithelial and stromal compartments, which has been reported to promote tumor progression by remodeling the extracellular matrix to enhance invasion and angiogenesis, releasing soluble factors and disarming the antitumor immune surveillance (3). Understanding the competing interactions between the several pro- and antitumorigenic components that shape the complex milieu of the tumor microenvironment, could lead to more integral approaches for cancer treatment (4).

Chronic inflammation has been associated with a high cancer incidence (5), providing clear evidence that a deregulated microenvironment affects tumorigenesis. An inflammatory setting fosters tumor progression through a wide range of mechanisms and represents a decisive factor in its evolution (6, 7). Of note, inflammation-driven anatomic expansion and increased activation of the remodeled microvascular bed promotes angiogenesis and further influx of immune cells, which become codependent processes (8).

Several molecular pathways have been linked to cancer and inflammation (9). In particular, the enzyme heme oxygenase-1 (HO-1) is part of an endogenous defense system implicated in the

[1]Universidad de Buenos Aires (UBA), Facultad de Ciencias Exactas y Naturales (FCEN), Departamento de Química Biológica (QB), Laboratorio de Inflamación y Cáncer, Buenos Aires, Argentina. [2]Universidad de Buenos Aires (UBA), Facultad de Ciencias Exactas y Naturales (FCEN), Departamento de Química Biológica (QB), Laboratorio de Glico-Oncología Molecular y Funcional, Buenos Aires, Argentina. [3]CONICET – Universidad de Buenos Aires (UBA), Instituto de Química Biológica de la Facultad de Ciencias Exactas y Naturales (IQUIBICEN), Buenos Aires, Argentina. [4]Department of Pathology, Institute of Oncological Studies, National Academy of Medicine, Buenos Aires, Argentina. [5]Fundación Instituto Leloir (FIL) – IIBBA – CONICET, Buenos Aires, Argentina. [6]Aston Medical Research Institute, Aston Medical School, University of Aston, Birmingham, United Kingdom. [7]Department of Genitourinary Medical Oncology and the David H. Koch Center for Applied Research of Genitourinary Cancers, The University of Texas MD Anderson Cancer Center, Houston, Texas. [8]Laboratorio de Inmunopatología, Instituto de Biología y Medicina Experimental (IBYME), CONICET, Buenos Aires, Argentina. [9]Universidad de Buenos Aires, Facultad de Ciencias Exactas y Naturales, Buenos Aires, Argentina. [10]Departamento de Ciencias Básicas, Universidad Nacional de Luján, Buenos Aires, Argentina.

**Note:** Supplementary data for this article are available at Clinical Cancer Research Online (http://clincancerres.aacrjournals.org/).

D.J. Laderach and E.S. Vazquez share senior authorship of this article.

**Corresponding Authors:** Elba S. Vazquez, Intendente Guiraldes 2160, Piso 4, Pabellón II, Ciudad Universitaria (1428), Buenos Aires, Argentina. Phone: 5411-4576-3300; Fax: 5411-4576-3342; E-mail: elba@qb.fcen.uba.ar; and Diego J. Laderach, Intendente Guiraldes 2160, Piso 4, Pabellón II, Ciudad Universitaria (1428), Buenos Aires, Argentina. Phone: 5411-4576-3300; diegoladerach@qb.fcen.uba.ar

**doi:** 10.1158/1078-0432.CCR-17-0112

## Translational Relevance

Prostate cancer remains a major health care problem worldwide. Although most current therapies against this disease are designed to target the tumor cells themselves, the surrounding microenvironment plays a leading role in enabling the growth and dissemination of the tumor. Using a fully immunocompetent murine model, our results reveal how stromal conditioning with hemin, a well-known inducer of heme oxygenase-1 (HO-1), limits prostate cancer development by targeting both tumor vascularization and the cytotoxic T-cell responses. Taken altogether, these data showcase a novel function of an already human-used drug as a means to boost the endogenous antitumor response.

homeostatic response (10, 11). The intrinsic effect of HO-1 on tumor cells in different cancer models has been extensively addressed (12, 13). Furthermore, data are available from a wide spectrum of physiopathologic conditions that link HO-1 to modulation of angiogenesis and the immune function, 2 hallmarks of cancer (7).

In prostate cancer, we have demonstrated that HO-1–overexpressing human xenografts generated in nude mice show impaired growth (14) and angiogenesis (15) and that this protein modifies the bone microenvironment modulating prostate cancer bone metastasis (16). We recently reported that HO-1 shapes cell–cell interactions, favoring a less aggressive phenotype (17, 18). Moreover, HO-1 inhibited relevant pathways implicated in prostate tumorigenesis (16, 19). Other groups have also provided evidence showing that HO-1 finely tunes prostate cancer progression by exerting both protumor (20, 21) and antitumor roles (22). However, despite considerable evidence regarding the role of this enzyme in the epithelial tumor cell compartment, its role in the tumor microenvironment still remains elusive.

Conditioning strategies constitute a relatively unexplored and exciting opportunity to shape tumor fate by targeting the tumor microenvironment. In this study, we assessed whether conditioning with hemin, known to induce HO-1, affects prostate cancer development using an immunocompetent murine model. Hemin treatment prior to tumor challenge resulted in a significant increase in tumor latency by targeting both tumor vascularization and cytotoxic T-cell responses. Taken altogether, these data showcase a novel function of an already human-used drug as a treatment to boost the endogenous antitumor response.

## Materials and Methods

### Cell culture

TRAMP-C1 cells (T-C1; ATCC) were cultured in DMEM (Invitrogen), 10% FBS (Gibco), antibiotic–antimycotic (Gibco), and insulin (5 μg/mL). Cell morphology, androgen sensitivity, and mycoplasma contamination were routinely assessed. Human umbilical vein endothelial cells (HUVEC; Lonza) were maintained in EGM-2 (Lonza). Bovine aortic endothelial cells (BAECs) were provided by M.T. Elola (IQUIFIB, UBA-CONICET; UBA-FFyB-QB; Buenos Aires, Argentina) and cultured as described previously (23). Lymph node cell primary cultures were carried out in RPMI1640 (Invitrogen) containing 10% FBS (PAA), antibiotics, 2 mmol/L L-glutamine, and $2 \times 10^{-5}$ mol/L β-mercaptoethanol. Hemin (Sigma-Aldrich) was dissolved in 1 mol/L Tris-HCl, pH 8, 0.5 mol/L NaOH, and PBS. This solution was 22-μm filtered and diluted in PBS or culture media.

### Animals

Animal procedures complied with institutional guidelines. Six- to 8-week-old male C57BL/6 mice were housed in the animal facility of the FCEN-UBA. *Foxn1*$^{nu}$ mice were acquired from the animal facility of UNLP. T-cell receptor transgenic mice specific for H-2Kb $OVA_{257\text{-}264}$ (male OT-1 mice) were raised and tested at FIL-IIBBA-CONICET.

### Hemin conditioning and subcutaneous tumor model

Mice were subcutaneously injected with hemin (200 μL, 30 μmol/L) on days −8, −5, and −1 prior to challenge with $2 \times 10^6$ T-C1 cells on the same flank. Alternatively, hemin was administered on the contralateral flank when specified. Control littermates were injected with PBS. T-C1 cells were subcutaneously injected in Matrigel (4–5 mg/mL; Corning). No changes in weight were detected. Euthanasia was practiced at the most when tumor volume reached 1,500 $mm^3$. Tumor size was calculated as $W^2 \times L/2$ ($W$ = width, $L$ = length). Tumor volume was normalized to that at the start day of exponential growth.

### Real-time reverse transcription PCR

Transcriptional profile was analyzed in T-C1 tumor samples and lymph node samples, as described previously (23). Primers are listed in Supplementary Table S1. Human *PPIA*, murine *Rplp0*, and bovine *GAPDH* were used as internal reference genes.

### Histologic analysis

Sections obtained from paraffin-embedded tissues were stained according to Masson trichrome technique or subjected to IHC, as described previously (14, 23), using anti-HO-1 (ab13243, Abcam), anti-Gal-1 (H-45, Santa Cruz Biotechnology, Inc.), and anti-CD31 (D8V9E, Cell Signaling Technology) antibodies. Blinded qualitative studies were carried out by a pathologist (R.P. Meiss).

### Prostate cancer patient-derived xenografts and tissue microarray technology

Patient-derived xenograft (PDX) were generated at MD Anderson Cancer Center (Houston, TX; ref. 24) to prepare the TMA ($n$ = 50). IHC was carried out and blinded semiquantitative studies were performed (R.P. Meiss): 0, no staining; 1, 2, and 3, low, mild, and high staining, respectively. Scores of individual blokes corresponding to the same PDX were averaged.

### Tubulogenesis assay

Eighty-percent confluent T-C1 cells were cultured for 24 hours in a 1:5 diluted growth media. Conditioned media (CM) was harvested and filtered. Sixty microliters of growth factor–reduced Matrigel was plated in a 96-well plate and incubated at 37°C for 15 minutes. A total of $12.5 \times 10^3$ hemin-treated (50 μmol/L, 8 hours) or control HUVECs were plated on the Matrigel in the presence of control or T-C1–derived CM. Positive control wells were seeded in EGM-2 medium. Endothelial tube formation was evaluated after 18 hours. Five fields per well were photographed. AdobePhotoshop-processed photographs were evaluated using the NIH ImageJ Angiogenesis Analyzer Plug-in.

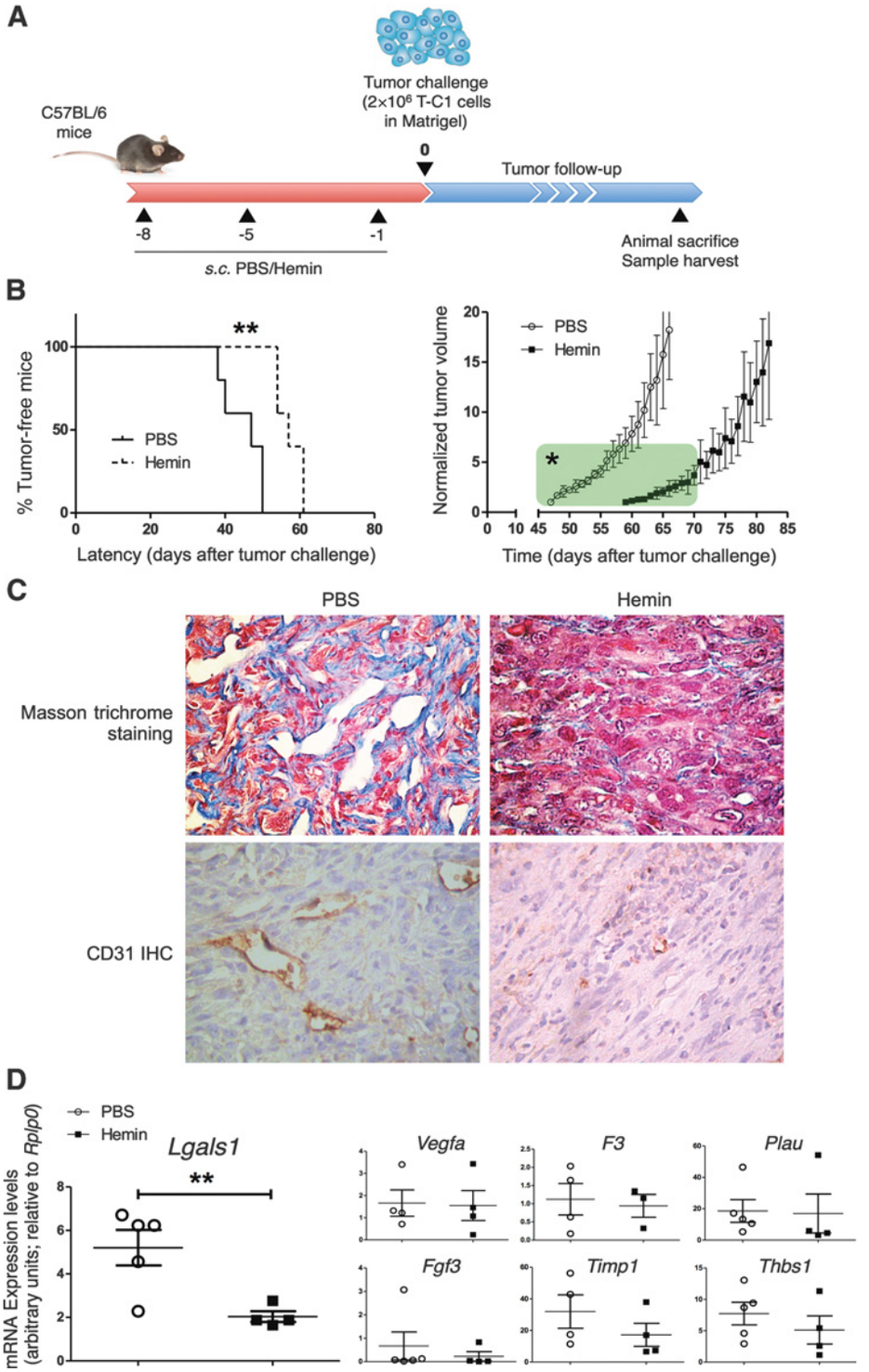


**Figure 1.**
Hemin conditioning blunts prostate cancer tumor development. C57BL/6 mice ($n = 5$) were subcutaneously injected with hemin (200 µL, 30 µmol/L) on days –8, –5, and –1 prior to tumor challenge on the same flank ($2 \times 10^6$ T-C1 cells in Matrigel). Control littermates were injected with PBS. In all cases, empty circles represent control mice and filled circles depict hemin-conditioned mice. **A,** Schematic representation of the experimental protocol. **B,** Tumor growth follow-up. Left, the percentage of tumor-free mice along the course of the experiment. Solid line, control animals; dashed line, hemin pretreated mice. **, $P < 0.01$, Mantel–Cox test. Right, normalized tumor volume evolution. *, $P < 0.05$ when comparing data contained in the shadowed box; Student $t$ test. **C,** Histologic analysis of paraffin-embedded tumor sections obtained from control or hemin pretreated mice at the experimental endpoint. Masson trichrome staining and CD31 IHC analysis were performed. Original magnification, ×400. **D,** Transcriptional analysis of several angiogenesis-related genes. qRT-PCR was performed from tumor total RNA and the relative expression of the following genes was assessed: vascular endothelial growth factor-A (*Vegfa*), thrombosplastin (*F3*), plasminogen activator, urokinase (*Plau*), fibroblast growth factor-2 (*Fgf2*), TIMP metallopeptidase inhibitor-I (*Timp1*), thrombospondin (*Thbs1*), and galectin-1 (*Lgals1*). The murine acidic ribosomal protein P0 gene *Rplp0* was used as an internal reference gene (**, $P < 0.01$, Student $t$ test).

### Apoptosis assay

BAECs were treated with hemin (50 µmol/L, 8 hours), washed, and subsequently cultured for 16 hours in a 1:5 diluted growth media containing recombinant Gal-1 (ref. 25; 0, 2.25, 4.5, and 9 µmol/L). Detached and adherent cells were photographed, harvested (TripLE Express, Thermo Fisher), and stained with FITC-Annexin-V (Apoptosis Detection kit, BD Pharmingen) and propidium iodine (Sigma), followed by flow cytometry.

### Wound healing assay

HUVECs were treated with hemin (50 µmol/L, 8 hours), washed, and subsequently cultured for 24 hours in a 1:5 diluted

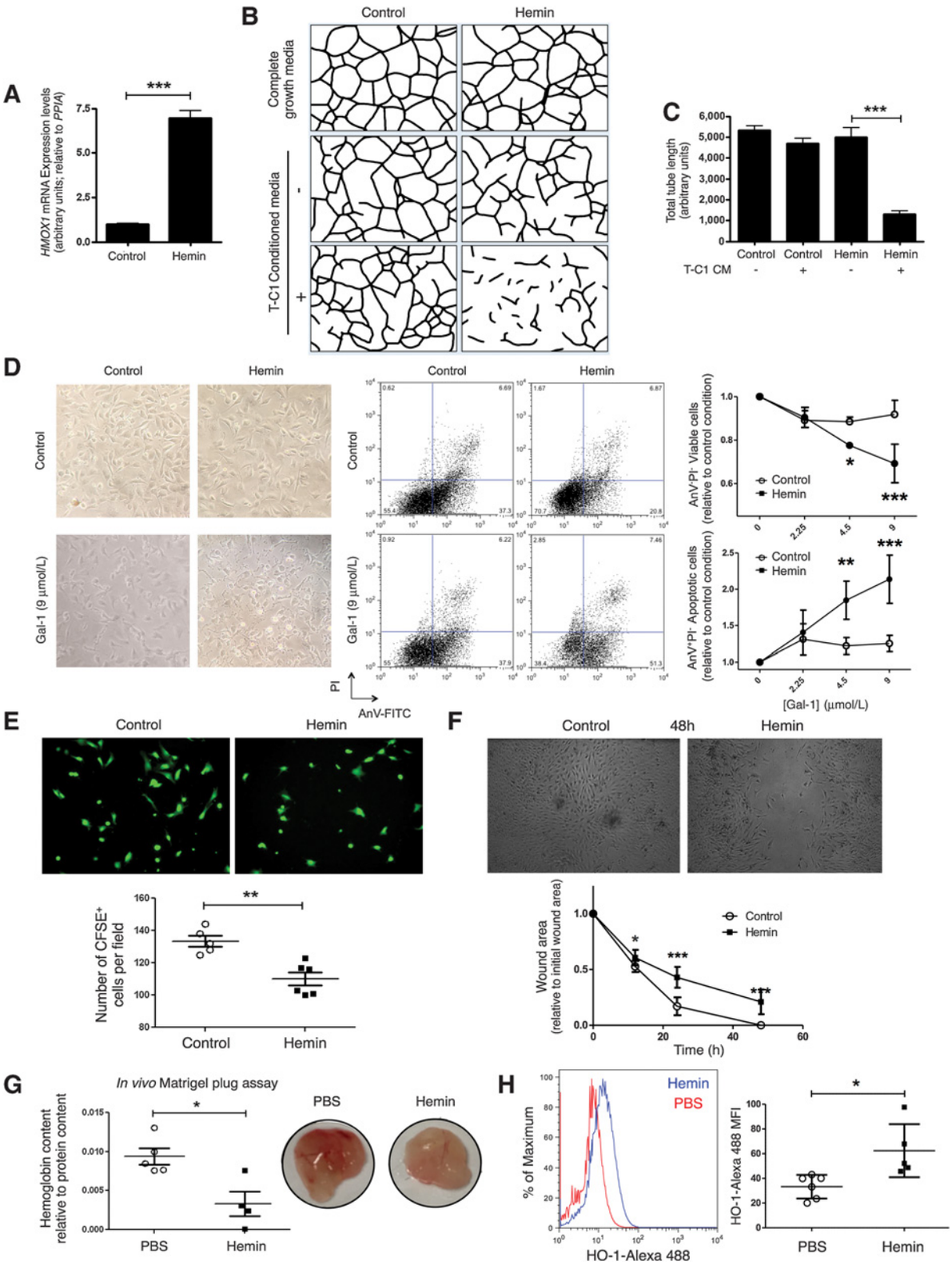

growth media. CM was harvested and filtered. Confluent T-C1 cells were washed and serum-starved for 8 hours. A 1-mm-wide scratch was made across the cell layer and, after washing with serum-free medium twice, hemin-treated or control HUVEC CM was added, and plates were photographed immediately and after incubation (12, 24, 48 hours) at the identical location of initial image. Wound area was quantified using NIH ImageJ.

### Tumor-to-endothelium adhesion assay

Eighty-percent confluent HUVECs were treated with hemin (50 μmol/L, 8 hours) and subsequently washed. A total of $3 \times 10^4$ CFSE-labeled T-C1 cells (2.5 μmol/L, 5 minutes, $1 \times 10^6$ cells/mL in PBS 1% FBS; Sigma) were added. After incubating 2 hours at 37°C, unattached cells were washed away, and 3 different fields of each well were photographed. Cells were counted using the NIH ImageJ Cell Counter Plug-in.

### *In vivo* Matrigel plug assay

A total of $2 \times 10^6$ T-C1 cells in 500 μL of Matrigel (4–5 mg/mL) were subcutaneously injected into mice following hemin conditioning. Five days later, Matrigel plugs were harvested and photographed. Plugs were homogenized in $H_2O$ and cleared by centrifugation. Hemoglobin and total protein content were determined using the Drabkin reagent (WienerLab) and the Pierce BCA Protein Assay kit (Thermo Scientific).

### Lymphocyte proliferation and degranulation assays

For T-cell proliferation assays, $5 \times 10^5$ CFSE-stained murine lymph node cells (2.5 μmol/L, 5 minutes) were seeded in a 96-well U-bottomed plate. Hemin was added into culture (18.75, 37.5, and 75 μmol/L). A total of $1 \times 10^4$ mitomycin-arrested T-C1 cells (3-hour treatment, 10 μg/mL; Sigma) were added into cultures to mimic a tumor microenvironment. For T-cell degranulation, cells were stimulated with coated anti-CD3 antibody (145-2C11 hybridoma; 1 μg/mL, 12 hours) and anti-CD107a was added (1 hour, 37°C; 1D4B, BD Pharmingen) followed by an additional 4-hour culture with monensin (3 μmol/L; BD Pharmingen). Spontaneous expression of CD107a was also evaluated. For T-cell proliferation, cells were stimulated with coated anti-CD3 antibody (1 μg/mL, 72 hours) and proliferation assessed by CFSE dilution. Cells were stained for CD8 (53-6.7, BD Pharmingen) in staining buffer (PBS 1% FBS, 0.01% sodium azide; 30 minutes on ice). HO-1 induction was confirmed by intracytoplasmatic staining (ab13248; Abcam). FACS was performed in a FACSAria (BD Biosciences) using the FlowJo software.

### *In vivo* cytotoxic T-lymphocyte assay

WT C57BL/6 mice were irradiated (1 Gy; $^{137}$cesium source; Cebirsa), transferred with $3 \times 10^6$ OT-1 lymph node cells, and subcutaneously injected with hemin on a daily basis for 3 days. On the next day, freshly isolated WT C57BL/6 spleen cells were obtained by mechanical disruption, and erythrocytes were lysed. Splenocytes were stained with CFSE (5 μmol/L or 0.5 μmol/L). $CFSE_{dim}$ cells were incubated with OVA-derived SIINFEKL peptide (10 μg/mL, 30 minutes, 37°C; Invivogen); $CFSE_{bright}$ cells were exposed to the vehicle alone. Mice were transferred with a 1:1 mix of $CFSE_{dim\text{-}OVA}$ and $CFSE_{bright\text{-}ctrl}$ cells ($2 \times 10^6$ cells, 100 μL). After 16 hours, spleens were processed for FACS analysis. Alternatively, hemin treatment was carried out *ex vivo* (75 μmol/L, 8 hours) prior to adoptive transfer. Mice with no previous transfer of OT-1 lymph node cells were used as a control to calculate specific cytotoxicity as follows: $SC = [1 - (\%CFSE_{dim\text{-}OVA}/\%CFSE_{bright\text{-}ctrl})_{transferred\ mice} \times (\%CFSE_{bright\text{-}ctrl}/\%CFSE_{dim\text{-}OVA})_{nontransferred\ mice}] \times 100$.

### Flow cytometric analysis of murine samples

Tumor, spleen, tumor-draining lymph node (TDLN; axillary, brachial, and inguinal), and blood vessel–containing tissue samples were harvested and single-cell suspensions were obtained by mechanical disruption. Tumor samples were previously disaggregated with Collagenase type IV (1 mg/mL, 1 hour, 37°C; Sigma). Cells were stained and analyzed by FACS. Anti-CD3-FITC (17A2; BD Biosciences), anti-CD11b-PE (M 1/70; BD Biosciences), anti-Gr-1-FITC (RB6-8CS; BD Biosciences), anti-CD31 (390, BD Pharmingen), anti-HO-1, goat-anti-rat Ig-PE (550767, BD Biosciences) goat-anti-mouse IgG1-Alexa488 (A21121, Thermo Fisher Scientific) were used.

### Bioinformatics analysis

We searched Oncomine (26) to identify human expression microarray datasets that compare prostate adenocarcinoma versus normal gland. Supplementary Table S2 shows information about these datasets. Cited literature was reviewed to confirm that the analysis was as documented.

**Figure 2.**

Hemin remodels the interaction between the endothelial cell and the prostate tumor cell. **A,** Expression of *HMOX1* mRNA levels in control and hemin-treated HUVEC (50 μmol/L, 8 hours), as determined by qRT-PCR 16 hours after hemin treatment. Human cyclophilin A gene *PPIA* was used as an internal reference gene. ***, $P < 0.001$; $n = 3$; Student *t* test. **B,** *In vitro* tube formation using control or hemin-treated HUVECs in the absence or presence of T-C1–conditioned media. Binary tree structures were obtained from original microscopic photographs. Complete growth media served as a positive control. Figure depicts one representative out of 3 independent experiments. **C,** Total tube length was quantified. ***, $P < 0.001$; $n = 3$; two-way ANOVA. **D,** Gal-1–induced apoptosis was assessed on both control and hemin pretreated endothelial cells, by measuring Annexin-V (An-V) binding and propidium iodine (PI) staining followed by flow cytometry. Left, representative photographs for the different experimental conditions (original magnification ×100). The central panel shows representative dot plots obtained by flow cytometry for the different experimental conditions. Right, quantification of viable and early apoptotic cells. *, $P < 0.05$; **, $P < 0.01$; ***, $P < 0.001$; $n = 4$; two-way ANOVA. **E,** The effect of control or hemin-treated HUVEC conditioned media on TC-1 migration was evaluated through a wound scratch assay. Photographs taken 48 hours after scratch show representative images. Wound area was quantified 12, 24, and 48 hours after scratch (right). *, $P < 0.05$; ***, $P < 0.001$; $n = 3$; Student *t* test. **F,** T-C1 adhesion to hemin pretreated HUVEC was assessed by adding CFSE-labeled T-C1 cells to an endothelial monolayer. After 2 hours of incubation at 37°C, detached cells were washed out with PBS and adhered cells were counted under an inverted fluorescent microscope. Photographs show representative images. Right, number of labeled T-C1 cells per field. **, $P < 0.01$; $n = 3$; Student *t* test. **G,** T-C1 cells in Matrigel were subcutaneously injected into C57BL/6 mice following hemin conditioning ($n = 5$). Five days later, Matrigel plugs were harvested and photographed. Right, representative plugs. Once homogenized, hemoglobin and total protein content were determined. Left, hemoglobin content relative to total protein content. *, $P < 0.05$, Student *t* test. In all cases, empty circles represent control conditions and filled circles depict hemin treatments. **H,** Samples of blood vessel–containing tissue derived from the injected flank were retrieved on the day that mice would have been challenged with tumor cells, and CD31 and HO-1 expression levels were assessed by flow cytometry. Left, representative histogram per experimental condition. Right, the mean fluorescence intensity for each mouse (*, indicates $P < 0.05$; Student *t* test).

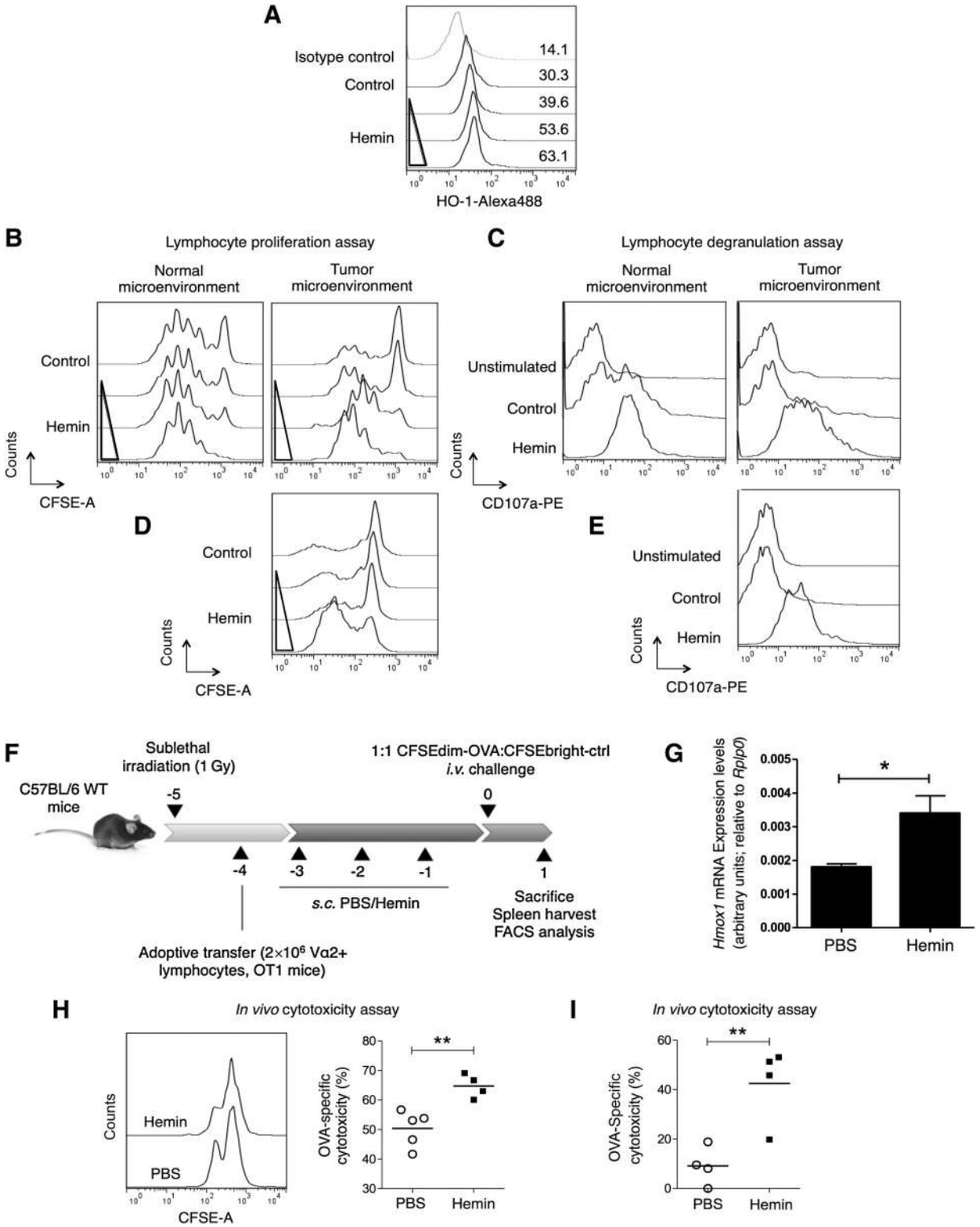


**Figure 3.**

Hemin enhances CD8$^+$ CTL responses. **A–E,** Results depict 1 representative of 3 independent experiments. **A,** Lymph node cells were cultured with hemin (8 hours; 18.75, 37.5, and 75 μmol/L) and HO-1 expression assessed by intracytoplasmatic staining; numbers indicate mean fluorescence intensity. **B,** CD8$^+$ T-cell proliferation in response to coated anti-CD3 antibody (1 μg/mL). T-C1 cells were added to mimic a tumor microenvironment. Cultures were treated with hemin (18.75, 37.5, and 75 μmol/L). CFSE dilution was assessed 72 hours poststimulation. (*Continued on the following page.*)

### Statistical analysis

At least 3 biological replicates (i.e., independent experiments) were carried out. Data represent mean ± SD. GraphPad software was used. Two groups were compared with the Student *t* test for unpaired data. Two-way ANOVA tests were used for multiple comparisons (with Tukey and Bonferroni *post hoc* tests). Nonparametric Mantel–Cox tests were carried out when comparing tumor-free mice curves. $P < 0.05$ was considered statistically significant.

## Results

### Hemin conditioning impairs prostate cancer development

Given the scarce prostate cancer preclinical models available allowing assessment of the whole tumor microenvironment, we used a syngeneic model based on the subcutaneous injection of T-C1 cells into C57BL/6 mice, previously standardized in our laboratory (27). TRAMP cells constitute the only murine prostate cancer cells lines appropriate for implantation into syngeneic immunocompetent mice. To study whether hemin conditioning influences tumor development, mice ($n = 5$) were subcutaneously injected with this agent (200 μL; 30 μmol/L) on days −8, −5, and −1 prior to tumor challenge on the same flank ($2 \times 10^6$ T-C1 cells in Matrigel; Fig. 1A). Control littermates ($n = 5$) were injected with saline. Hemin dosage was not arbitrary chosen, it was adapted from the dose used for human porphyria. Pharmacokinetics, pharmacodynamics, and toxicologic studies have been performed in animals prior to hemin acceptance for use in humans. Although tumors developed in all the mice, pretreatment resulted in a marked increase in tumor latency (57 ± 3 days in hemin-treated mice vs. 47 ± 5 days in control mice; Fig. 1B, left). Furthermore, initial growth rate was significantly reduced in hemin-treated animals (Fig. 1B, right). Tumor histologic analysis at the time of euthanasia showed lower number of blood vessels in the experimental group, as revealed by both trichrome staining and CD31 IHC (Fig. 1C). Evaluation of mediators typically involved in angiogenesis [VEGF-A, CD142, uPA, FGFb, TIMP-1, TSP-1, and galectin-1 (Gal-1)] revealed that only the Gal-1-coding mRNA (*Lgals1*) expression was significantly reduced in hemin-treated animals (Fig. 1D). Remarkably, our group and others have previously reported an upregulated expression of this lectin in human prostate cancer and its correlation with the tumor angiogenic phenotype (23, 28).

### Hemin conditioning reprograms the angiogenic switch in prostate cancer

Considering our previous findings that HO-1 and Gal-1 expression play a critical role in prostate cancer neovascularization (15, 23), we analyzed the effect of hemin on endothelial cells within a prostate tumor setting. HO-1 induction was confirmed by qRT-PCR (*Hmox1* mRNA; Fig. 2A). An *in vitro* tube formation assay was performed using hemin pretreated HUVECs, seeded onto Matrigel-coated wells in the presence or absence of T-C1–derived CM. Hemin pretreatment dramatically inhibited tubulogenesis only in the presence of tumor CM (Fig. 2B; Supplementary Fig. S1A), as reflected by a significant reduction of total tube length (Fig. 2C) and the number of master segments and tube joints in this experimental condition (Supplementary Fig. S1B). Importantly, the tube network was not hindered both in complete growth media and in the absence of T-C1–derived CM, confirming HUVEC viability is not significantly affected by hemin pretreatment. To evaluate the role of Gal-1, we carried out an apoptosis assay in the presence of the recombinant lectin. While control cells did not show Gal-1–induced apoptosis, hemin-treated endothelial cells were significantly more susceptible to cell death in a Gal-1 dose-dependent fashion (Fig. 2D). Of note, hemin-treated cells did not show any significant differences in terms of basal cell death when compared with control cells. The increase in endothelial cell death was further supported by a significant decrease in CD146 mRNA levels (Supplementary Fig. S2), a coreceptor for VEGFR-2 and a decoy receptor for Gal-1 (29, 30). We next studied whether hemin conditioning influences the crosstalk between tumor and endothelial cells. T-C1 cell motility was significantly impaired when a wound-healing assay was performed in the presence of hemin pretreated HUVEC CM (Fig. 2E). Tumor cell adhesion to endothelial cells was severely reduced when HUVECs were pretreated with hemin (Fig. 2F). We ruled out there were hemin traces in the CM by assessing *HMOX1* mRNA expression levels in T-C1 that had been exposed, and detected no significant differences (data not shown). Collectively, these findings suggest that hemin conditioning remodels the endothelial compartment and negatively regulates interactions between endothelial and tumor cells. To assess whether hemin pretreatment is implicated in tumor neovascularization *in vivo*, we performed a Matrigel plug assay. C57BL/6 mice ($n = 5$) were subjected to our hemin-conditioning protocol before being injected with T-C1 cells in Matrigel. Control mice ($n = 5$) were injected with saline-containing Matrigel. After 5 days, plugs were harvested and hemoglobin content was determined. In keeping with our *in vitro* findings, hemin pretreatment significantly inhibited vascularization *in vivo* (Fig. 2G). In summary, hemin conditioning impacts upon the angiogenic process, probably accounting for tumor growth inhibition (Fig. 1B). To verify that hemin conditioning induces HO-1 expression in endothelial cells, on the day that mice would have been challenged with tumor cells, we collected samples of blood vessel–containing tissue from the same



(*Continued.*) **C,** $CD8^+$ T-cell degranulation in response to coated anti-CD3 antibody (1 μg/mL) was measured by CD107a mobilization to the plasma membrane. Cells were stimulated in the presence or absence of hemin (12 hours; 75 μmol/L) and stained for extracellular CD107a. **D** and **E,** Lymph node cells were cocultured with T-C1 cells for 24 hours in an anti-CD3–coated well (1 μg/mL). Hemin (18.75, 37.5, and 75 μmol/L) was then added and proliferation was measured after 72 hours as described previously. Alternatively, degranulation was measured after 12 hours as described previously. **F–H,** *In vivo* $CD8^+$ cytotoxicity assays. Empty circles represent control mice; filled circles depict hemin-conditioned mice. **F,** Schematic representation of the *in vivo* OVA-specific cytotoxicity assay. **G,** Expression of *Hmox1* mRNA levels in inguinal, brachial, and axillary lymph nodes retrieved from both hemin-treated and control animals, as determined by qRT-PCR. Samples were collected on the day following the last subcutaneous injection. *, $P < 0.05$; Student *t* test. **H,** OT-1 lymph node cell-transferred mice ($n = 5$) were treated with hemin and subsequently challenged with a mix of $CFSE_{dim\text{-}OVA}$ and $CFSE_{bright\text{-}ctrl}$ cells (1:1). After 16 hours, their relative proportion was evaluated by flow cytometry of splenic homogenates (left). Right, percentage of OVA-specific cytotoxicity. **, $P < 0.01$, Student *t* test. **I,** Hemin treatment was performed *ex vivo* (8 hours; 75 μmol/L) prior to adoptive transfer into nonirradiated C57BL/6 mice ($n = 5$). Animals were subsequently challenged with $CFSE_{dim\text{-}OVA}$ and $CFSE_{bright\text{-}ctrl}$ cells and 16 hours later sacrificed for cytotoxicity analysis. The figure shows the percentage of OVA-specific cytotoxicity (**, $P < 0.01$, Student *t* test).

animal flank that had been previously injected with either PBS ($n = 6$) or hemin ($n = 5$). We subsequently assessed HO-1 expression in endothelial cells using FACS and we confirmed that hemin treatment *in vivo* results in increased HO-1 expression in $CD31^+$ cells (Fig. 2H).

### Hemin conditioning fosters $CD8^+$ T-cell responses

Both HO-1 and Gal-1 have been reported to play major roles in shaping antitumor responses (31, 32). We thus analyzed hemin effect upon the immune compartment by performing *in vitro* cocultures of lymph node cells isolated from C57BL/6 mice with syngeneic T-C1 cells. Hemin induced HO-1 in a dose-dependent fashion in $CD8^+$ cytotoxic T lymphocytes (CTLs), as determined by intracellular staining and flow cytometry (Fig. 3A). FACS analysis of cell division by CFSE staining demonstrated that hemin increases $CD8^+$ T-cell proliferation in a dose-dependent manner in response to polyclonal activation (Fig. 3B, left), even when cocultured with tumor cells (Fig. 3B, right). We also examined hemin effects on the cytotoxic potential of $CD8^+$ T cells, by measuring the expression of CD107a on the cell surface as a result of CTL degranulation. Hemin treatment resulted in enhanced CTL effector function both in normal and tumor microenvironments (Fig. 3C). To evaluate whether hemin also boosts the immune function in an established tumor immunosuppressive setting, lymph node cells and T-C1 cells were cocultured 24 hours prior to hemin addition. Hemin augmented $CD8^+$ T-cell proliferation and degranulation even under these experimental conditions (Fig. 3D and E), reverting tumor immunosuppression. To verify the relevance of these findings *in vivo*, we tested cytotoxicity following hemin conditioning by performing a CTL assay. $CD8^+$ T-cell effector function *in vivo* was determined by mixed transfer of OVA peptide–pulsed target cells with control cells into WT C57BL/6 mice previously transferred with OT-1–derived lymph node cells ($n = 5$; Fig. 3F). We confirmed that hemin treatment induced HO-1 expression at the transcriptional level in lymph node samples collected on the day that mice would have been transferred with the mix (Fig. 3G). The left panel of Fig. 3H shows representative results, where the relative frequencies between peptide-pulsed target cells and control cells were used as readouts of specific killing. The frequency of $CFSE_{dim\text{-}OVA}$ cells was reduced to a greater extent in hemin-treated mice compared with control littermates. OVA-specific cytotoxicity was significantly enhanced when transferred mice were subcutaneously treated with hemin prior to challenge with OVA-loaded cells (Fig. 3H, right). We next sought to determine whether hemin boosts antigen-specific cytotoxicity *in vivo* if OT-1 lymph node cells were treated *ex vivo* prior to adoptive transfer into WT C57BL/6 mice. Hemin-treated lymphocytes led to augmented OVA-specific cytotoxicity (Fig. 3I). Our results indicate that the sole exposure of lymph node cells to hemin boosts $CD8^+$-mediated cytotoxicity, which could account for tumor growth inhibition (Fig. 1B).

### Hemin conditioning targets the vascular and immunologic compartments and restrains prostate tumor development

To investigate whether hemin conditioning influences vascular and immunologic compartments at earlier stages of tumor development, tumor-bearing C57BL/6 mice ($n = 4$) were sacrificed when control mice exhibited tumors in their exponential growth phase, while hemin pretreated mice showed tumors in their initial growth steps. The frequency of $CD3^+CD8^+$ cells in hemin-conditioned mice was systemically increased, as determined by immunophenotyping the tumor, draining lymph nodes, and spleen (Fig. 4A). Furthermore, the frequency of regulatory $Gr\text{-}1^+CD11b^+$ myeloid cells in the tumor-draining lymph nodes was reduced in hemin pretreated mice compared with control animals (Fig. 4B), probably allowing a more effective antitumor immune response. Histologic analysis revealed that control tumors, but not tumors derived from hemin-conditioned mice, showed dilated blood vessels mimicking an angiomatous image (Fig. 4C, top and centre). In addition, hemin pretreated animals displayed tumors with reduced atypical mitotic figures when compared with control mice (Fig. 4C, bottom). IHC revealed lower levels of Gal-1 expression in tumors generated under hemin conditioning (Fig. 4D). These results further emphasize the essential role of the tumor microenvironment in governing the fate of tumor development. Considering the systemic changes in conditioned mice (Fig. 4A and B), we next evaluated whether hemin exerts an antitumor effect when injected at a site other than the flank subsequently challenged with the tumor cells. Similar to hemin conditioning on the ipsilateral flank, its administration on the contralateral flank also led to a significant increase in tumor latency ($45 \pm 5$ days in control mice, $n = 8$; $56 \pm 3$ days in ipsilateral conditioned animals, $n = 10$; and $55 \pm 2$ days in the contralateral-conditioned group, $n = 5$; Fig. 4E). No significant differences were found between both conditioning strategies in terms of tumor latency, suggesting both treatments had a similar antitumor effect. Furthermore, in an effort to elucidate the relative contribution of the vascular and immune compartments, we tested whether hemin conditioning was able to modulate tumor development in athymic nude mice. Tumor latency and growth did not significantly differ when comparing hemin-conditioned animals with control mice (Fig. 4F), confirming that the immune system is required to target prostate cancer tumors in our experimental model.

### Bioinformatic analysis of human prostate adenocarcinoma microarray datasets

To address potential clinical implications of elevated HO-1 expression in human prostate tumor samples, we searched the microarray database Oncomine (26). We found 16 gene expression microarray datasets comparing prostate adenocarcinoma versus normal prostate tissue that met our eligibility criteria (Supplementary Table S2). Only 4 datasets presented increased expression for *HMOX1* mRNA with $P < 0.05$ (Table 1), in which only 1 of these datasets showed fold induction greater than 1.5. These results support the idea that HO-1 expression is not associated to prostate carcinogenesis. Given the small *P* values obtained for these 4 datasets ($n = 122$, $n = 112$, $n = 150$, $n = 19$; refer to Supplementary Table S2), we extended our analysis to assess the expression levels for *LGALS1*. Table 1 sums up the results obtained with all the datasets, whereas Supplementary Fig. S3 depicts representative results obtained when assessing Grasso Prostate Statistics (33). Interestingly, the expression profile for *LGALS1* showed significant downregulation for prostate adenocarcinoma versus normal gland in samples where *HMOX1* was upregulated (Table 1; Supplementary Fig. S3). We assessed in these same datasets the expression profiles of different angiogenesis-related genes (*CD34*, *FLT1*, *FLT4*, *KDR*, *VEGFA*, and *VEGFC*). Accordingly, their expression levels were downregulated for the prostate adenocarcinoma versus normal gland comparisons in which *HMOX1* was upregulated (Table 1; Supplementary Fig. S3). On the contrary, these datasets with

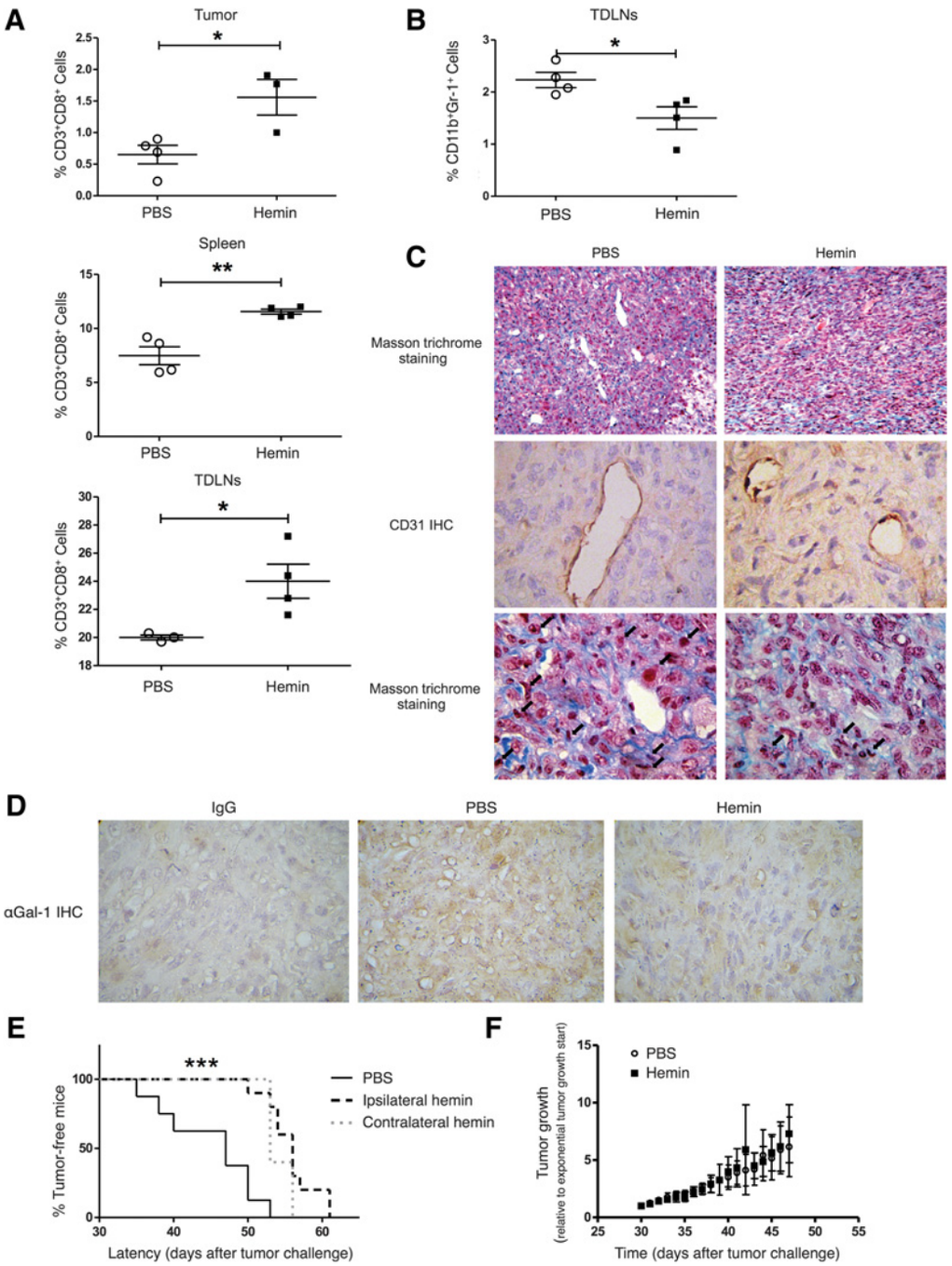


**Figure 4.**

Hemin conditioning shapes immunologic and vascular compartments and restrains prostate tumor growth. **A–D,** T-C1 tumor-bearing mice ($n = 4$) were sacrificed when control mice exhibited tumors in their exponential growth phase while hemin pretreated mice showed tumors in their initial growth steps. In all cases, empty circles represent control mice and filled circles depict hemin-conditioned mice. **A,** Tumor, spleen and tumor-draining lymph node (TDLN) samples were evaluated for $CD8^+$ T-cell frequency using flow cytometry. *, $P < 0.05$; **, $P < 0.01$, Student $t$ test. **B,** TDLN samples were assessed for $CD11b^+Gr\text{-}1^+$ cell frequency using flow cytometry; *, $P < 0.05$; Student $t$ test. **C,** Histologic analysis of paraffin-embedded tumor sections obtained from control or hemin pretreated mice. Masson trichrome staining and CD31 IHC analysis were performed. Top, original magnification, ×100; center and bottom, original magnification, ×400; arrows depict atypical mitotic figures. **D,** IHC staining against Gal-1 performed on paraffin-embedded tumor sections obtained from control or hemin pretreated mice. IgG refers to the control staining with rabbit preimmune sera. Original magnification, ×400. **E,** C57BL/6 mice challenged with T-C1 on the right flank were previously conditioned with hemin either on the same or the opposite flank (ipsilateral, $n = 10$; and contralateral flank, $n = 5$; respectively). Control littermates were injected with PBS on the same flank ($n = 8$). Figure shows the percentage of tumor-free mice along the course of the experiment. Solid line, control condition; black dashed line, hemin conditioning on the ipsilateral flank; gray dashed line, hemin conditioning on the contralateral flank. ***, $P < 0.001$, Mantel–Cox test. **F,** Athymic nude mice ($n = 5$) were subcutaneously injected with hemin prior to tumor challenge on the same flank. Control littermates were injected with PBS. Normalized tumor volume evolution is shown; empty circles represent control mice and filled circles depict hemin preconditioned mice.

**Table 1.** Summary table of results obtained for each database using Oncomine

| | *HMOX1* | *LGALS1* | *CD34* | *FLT1* | *FLT4* | *KDR* | *VEGFA* | *VEGFC* | *VCAM1* | *CD28* | *CD80* | *CD86* |
|---|---|---|---|---|---|---|---|---|---|---|---|---|
| Grasso et al. | 1.295<br>0.033<br>Top 25% | −1.708<br>7.23E−06<br>Top 7 | −1.179<br>0.045<br>Top 31% | −1.999<br>0.01<br>Top 23% | −1.214<br>0.007<br>Top 22% | | −1.656<br>0.008<br>Top 22% | −1.431<br>4.18E−06<br>Top 7% | 1.267<br>0.034<br>Top 25% | 1.373<br>0.036<br>Top 26% | 1.428<br>0.004<br>Top 15% | 4.127<br>9.52E−04<br>Top 12% |
| Varambally et al. | 2.292<br>0.002<br>Top 3% | −1.511<br>0.03<br>Top 19% | | −1.731<br>0.01<br>Top 11% | | | −1.975<br>0.009<br>Top 11% | −1.254<br>0.043<br>Top 22% | | 2.245<br>0.003<br>Top 4% | 1.21<br>0.244<br>Top 40% | 2.442<br>0.0071<br>Top 19% |
| Taylor et al. | 1.078<br>0.019<br>Top 19% | −1.548<br>0.019<br>Top 2% | −1.093<br>0.022<br>Top 19% | | | −1.127<br>0.042<br>Top 21% | −1.272<br>0.007<br>Top 15% | | 1.232<br>0.002<br>Top 9% | 1.109<br>4.31E−04<br>Top 4% | 1.144<br>3.19E−04<br>Top 6% | 1.138<br>1.26E−04<br>Top 5% |
| Lapointe et al. | 1.188<br>2.65E−04<br>Top 13% | | −1.249<br>0.005<br>Top 21% | −1.432<br>4.19E−04<br>Top 16% | | | −1.55<br>3.26E−06<br>Top 9% | | | 1.009<br>0.46<br>Top 58% | 1.035<br>0.298<br>Top 52% | 1.041<br>0.292<br>Top 52% |

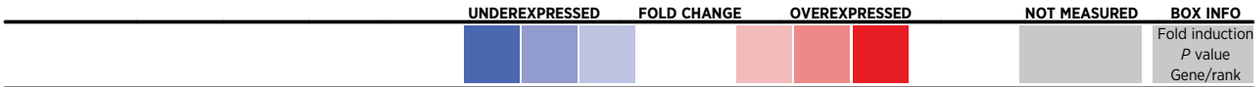


NOTE: Table depicts gene name, fold induction (adenocarcinoma vs. normal gland), *P* value, and gene rank. Bottom panel shows a heatmap indicating the level of expression for each gene in each study (blue, underexpressed; red, overexpressed).

increased expression of *HMOX1* also exhibited *VCAM1*, *CD28*, *CD80*, and *CD86* upregulation in prostate adenocarcinoma compared with the normal gland (Table 1; Supplementary Fig. S3). Interestingly, more intense lymphocyte infiltration was observed in tumors with elevated VCAM-1 (34). Furthermore, *CD28*, *CD80*, and *CD86* constitute key costimulatory molecules required to mount an effective immune response, and their elevated expression levels are indicative of T-cell activation. These results support the aforementioned findings and point toward a subset of patients who might respond to antiangiogenic and/or immunostimulatory therapy.

### Histologic analysis of HO-1 and Gal-1 in human prostate cancer PDXs

To further understand potential clinical implications, we screened a TMA containing 50 PDXs, each represented by PDXs grown in 3 different mice and 3 cores per tumor. These xenografts were derived from primary prostate cancer and metastatic sites and encompass samples of advanced prostate cancer with various histopathologic patterns. PDXs with heterogeneous staining between different cores or tumors for either HO-1 or Gal-1 were excluded from the analysis. PDXs were classified according to HO-1 immunostaining and we studied in detail those with low-to-intermediate HO-1 staining. This subset of PDXs displayed 2 clear clusters with either low or high Gal-1 immunostaining (Table 2). Those PDXs with mild HO-1 and low Gal-1 expression could be potentially more susceptible to an antiangiogenic and/or immune therapy, and could even benefit from the antiangiogenic properties of HO-1 induction (15).

## Discussion

Carcinogenesis is a multistep process encompassing mechanisms in both the epithelial cell and the surrounding tissue. Numerous signaling pathways are involved in the dynamic crosstalk between these compartments, and their deregulation influences disease initiation, progression, and patient prognosis (2). Novel experimental strategies have been designed to reeducate the microenvironment to shift the balance toward an antitumorigenic profile (4). Here we designed an experimental protocol using a murine model to shape the niche where prostate tumor cells are subsequently implanted (Fig. 1). We demonstrate for the first time that hemin conditioning remodels the bidirectional interactions between the tumor and the surrounding tissue, affects tumor neovascularization and immune function, and impairs tumor growth. Our results indicate that hemin conditioning acts, at least in part, through the inhibition of angiogenesis and the potentiation of tumor immunity, thus restraining prostate cancer development. Our findings also demonstrate that hemin modulated tumor development when injected on the contralateral flank (Fig. 4E). This strategy led to an increase in tumor latency that was comparable with that corresponding to ipsilateral hemin conditioning, further supporting potential novel therapeutic avenues for prostate cancer. Of note, hemin is approved for use in treatments against acute intermittent porphyria.

Angiogenesis is essential for tumor development given that proliferation of cancer cells, as well as their metastatic spread, rely on an adequate supply of both oxygen and nutrients and the removal of waste products. We demonstrate that hemin conditioning inhibits tumor-associated neovascularization *in vitro* and *in vivo* (Figs. 2 and 4). Hemin pretreatment of HUVEC dramatically hindered tubulogenesis only in the presence of tumor CM, suggesting hemin-treated HUVECs are refractory to proangiogenic tumor-derived factors. We also found that hemin conditioning limits the tumor angiogenic process *in vivo*. We have previously documented the antiangiogenic properties of HO-1 induction in the prostate cancer epithelial compartment (15). Moreover, this antiangiogenic effect was also demonstrated in pancreatic cancer by exogenous administration of the HO-1 metabolic product CO (35). In line with these observations, Ahmad and colleagues (36) recently reported that CO exposure inhibits VEGF-induced endothelial cell proliferation, migration, and capillary-like tube formation. Furthermore, in our preclinical model we found that Gal-1 expression was significantly reduced in tumors generated in hemin-treated mice. Our previous findings have shown that this lectin is highly expressed and regulated in the prostate cancer microenvironment and plays a major role in prostate cancer neovascularization (23). Notably, Croci and colleagues (25, 37) elegantly demonstrated the existence of a glycosylation-based circuit in which Gal-1 interaction with VEGFR2 mimics VEGF-A function and induces angiogenesis. Here we confirmed that Gal-1 promotes the formation of tube-like structures *in vitro*. Strikingly, hemin treatment sensitized endothelial cells to apoptosis in a Gal-1–dependent dose (Fig. 2). It has been previously reported that

**Table 2.** Tissue microarray data corresponding to PDXs with low-to-intermediate staining for HO-1

| PDX | | HO-1 expression | Gal-1 expression | Histopathology of human tumor of origin | Tumor site |
|---|---|---|---|---|---|
| MDA PCa 144 (3 PDXs from different areas of the same tumor) | MDA PCa 144-13 | 0.5 to 1.0 | 0.0 | Mixed adenocarcinoma and small-cell carcinoma with neuroendocrine differentiation | Local extension of prostate cancer to bladder |
| | MDA PCa 144-23 | 1.5 | 0.0 | Mixed adenocarcinoma and small-cell carcinoma with neuroendocrine differentiation | Local extension of prostate cancer to rectal wall |
| | MDA PCa 144-20 | 1.5 | 0.2 | Mixed adenocarcinoma and small-cell carcinoma with neuroendocrine differentiation | Local extension of prostate cancer to rectal wall |
| MDA PCa 155 (2 PDXs from different areas of the same tumor) | MDA PCa 155-2 | 1.5 | 0.3 | Poorly diferentiated carcinoma with neuroendocrine features | Local extension of prostate cancer to bladder neck |
| | MDA PCa 155-12 | 1.0 | 0.5 | Poorly diferentiated carcinoma with neuroendocrine features | Local extension of prostate cancer to bladder neck |
| | MDA PCa 160-29 | 0.9 | 0.6 | Prostatic sarcomatoid adenocarcinoma | Local extension of prostate cancer to intraprostatic urethra |
| MDA PCa 150 (2 PDXs from different areas of the same tumor) (*) | MDA PCa 150-5 | 1.0 | 0.7 | Poorly diferentiated carcinoma with Neuroendocrine features | Bone |
| | MDA PCa 150-3 | 1.5 | 0.8 | Poorly diferentiated carcinoma with neuroendocrine features | Bone |
| | MDA PCa 178-11 | 0.5 to 1.0 | 1.0 | Adenocarcinoma | Prostate |
| | MDA PCa 182-7 | 1.0 | 1.3 | Adenocarcinoma | Prostate |
| MDA PCa 150 (*) | MDA PCa 150-7 | 0.9 to 1.0 | 2.0 | Poorly diferentiated carcinoma with neuroendocrine features | Bone |
| | MDA PCa 166-1 | 1.3 | 2.0 | Adenocarcinoma | Local extension of prostate cancer to bladder neck |
| MDA PCa 153 (2 PDXs from different areas of the same tumor) | MDA PCa 153-14 | 1.0 to 1.8 | 2.1 | Adenocarcinoma with neuroendocrine differentiation | Thyroid |
| | MDA PCa 153-7 | 0.5 to 1.0 | 2.33 to 2.5 | Adenocarcinoma with neuroendocrine differentiation | Thyroid |
| | MDA PCa 188-2 | 0.5 | 2.2 | Adenocarcinoma | Local extension of prostate cancer to bladder |
| | MDA PCa 118b | 0.7 | 3.0 | Adenocarcinoma | Bone |
| | MDA PCa 180 | 1.5 | 3.0 | Adenocarcinoma | Local extension of prostate cancer to bladder |

NOTE: The table summarizes Gal-1 expression score, pathology diagnosis, anatomic description and tumor site, for each of the PDXs. Semiquantitative studies were carried out by a pathologist (R.P. Meiss); IHC staining was scored as follows: 0, no staining; 1, low staining; 2, mild staining; 3, high staining. PDXs are ordered vertically from top to bottom according to increasing Gal-1 expression.
Abbreviation: PCa, prostate cancer.

endothelial cells may undergo Gal-1–induced apoptosis when a potential coreceptor for VEGFR-2, CD146, is downregulated (29, 30); in this regard, we have indeed confirmed that hemin treatment upon endothelial cells inhibits CD146 expression. Moreover, taking into consideration the prolonged inhibition of Gal-1 expression in tumors evidencing impaired growth, our data might indicate that hemin conditioning remodels the endothelial compartment, affecting its interaction with the tumor cell. However, other studies have reported proangiogenic roles for HO-1 and its metabolic products in different cancer models and other pathologies (reviewed in refs. 12, 38), providing evidence of the inconsistent function of HO-1 in tumorigenesis and unveiling the complexity of the angiogenic process. Thus, the role of this protein is far from clear, but the general consensus of opinion is that its effect is highly dependent on tumor type, the trigger of tissue-specific signaling pathways, and the relative contribution of the enzymatic products and the noncanonical roles.

Nevertheless, simultaneous targeting of multiple components of the tumor microenvironment will be required to achieve a durable and efficient antitumor response. Our results indicate that hemin conditioning can also boost the immune response (Figs. 3 and 4). Hemin treatment resulted in enhanced $CD8^+$ T-cell proliferation and degranulation but, more importantly, we have provided strong evidence that subcutaneous administration of this agent augments *in vivo* antigen-specific cytotoxicity. Outstandingly, assays encompassing *ex vivo* lymph node hemin treatment prior to adoptive transfer supported hemin capacity to boost the $CD8^+$ cytotoxic function, which might in turn account for T-C1 tumor growth impairment. Indeed, we also observed a significant systemic expansion of $CD8^+$ T cells, suggesting that hemin conditioning may trigger long-term immunologic effects. Although the immunomodulatory function of HO-1 is well documented and its immunosuppressive role is widely accepted (31), relatively little attention has been paid to the effect of its substrate heme on the immune response. Remarkably, heme directly regulates various molecular and cellular processes, has been shown to act as a T-cell mitogen *in vitro* (39) and exerts mild proinflammatory responses encompassing the activation of macrophages and polymorphonuclear cells (40–42). Furthermore, recent findings have shown that oral administration of heme prior to induction of necrotizing enterocolitis decreased disease incidence and increased Treg/Teff ratios (43). In addition, Konrad and collaborators (44) demonstrated that topical administration of hemin was protective against pulmonary inflammation. Both studies have clearly associated the reported effects to HO-1 expression by using genetically modified animals. Two independent studies have shown that HO-1 expressed in macrophages may influence prostate cancer tumor fate and promote its growth (45, 46). Surprisingly, Jais and collaborators (47) claimed to have broken the HO-1 dogma by providing evidence of its proinflammatory role in hepatocytes and macrophages in the development of metabolic disease, using conditional genetically modified mice and patient datasets. In addition, Mashreghi and colleagues (48) showed that pharmacologic agents usually associated to HO-1 modulation have the capacity to shape the immune response independently of this protein. Thus, we may conclude that under our preclinical model hemin could trigger a complex immune response, characterized by augmented $CD8^+$ T-cell function. Finally, Gal-1 downregulation in tumors grown in hemin-conditioned animals might reflect potentiation of a tumor-specific immune response, as several findings indicate that this lectin plays critical protumorigenic roles within the tumor microenvironment, in part by suppressing T-cell–mediated cytotoxic responses (reviewed in refs. 32, 49). The relevance of the immune system in our experimental model becomes plainly evident when immunodeficient mice were conditioned with hemin prior to tumor challenge, as no significant differences were found. Although immunodeficient mice provide valuable information in cancer research, our findings add to cumulative data in literature that urge for fully immunocompetent and syngeneic animal models.

Finally, to assess the potential clinical implications of both HO-1 and Gal-1 in prostate cancer, we searched the cancer database Oncomine. Interestingly, a subset of patients displays mild upregulation of HO-1 with significantly lower expression for Gal-1, when comparing prostate adenocarcinoma versus normal gland (Table 1; Supplementary Fig. S3). This was further evidenced by the analysis of PDXs, which also showcased a subgroup with mild HO-1 and low Gal-1 expression (Table 2). This subpopulation could potentially be more susceptible to hemin treatment as an adjuvant therapy, maintaining Gal-1 expression levels severely low and, in combination with other antiangiogenic and/or immune therapies, might interrupt tumor growth and/or spread.

To summarize, our work provides evidence of the effect of hemin conditioning in both vascular and immune compartments, and its implications on prostate cancer development. Our strategy was conceived to remodel the environment to counteract the effects of tumor escape mechanisms. We speculate that novel therapeutic interventions should be designed to specifically target the reactive stroma. As mentioned above, we have previously shown that hemin treatment in prostate cancer cell lines does not have toxic effects and it even impairs proliferation, migration, and invasion *in vitro* and HO-1 overexpression leads to smaller and less vascularized tumors *in vivo* (14, 15). It should be noted that there is a considerable number of reports showcasing the protumor role of HO-1 in different types of cancer, even in prostate cancer (20, 21). Consequently, further study should be carried out to elucidate the HO-1 function in cancer development. We are currently developing new experimental strategies to assess hemin effects on prostate tumor progression *in vivo*, including intratumor injections and other means of specifically targeting immune and endothelial cells infiltrating the tumor. The results from this article provide a solid proof of concept to move forward in this direction.

## Disclosure of Potential Conflicts of Interest

No potential conflicts of interest were disclosed.

## Authors' Contributions

**Conception and design:** L. Gentilini, A. Ahmed, D. Compagno, D.J. Laderach, E.S. Vazquez

**Development of methodology:** F.M. Jaworski, R.P. Meiss, N.M. Navone, D. Compagno, D.J. Laderach

**Acquisition of data (provided animals, acquired and managed patients, provided facilities, etc.):** G. Gueron, R.P. Meiss, P.M. Berguer, D.J. Laderach, E.S. Vazquez

**Analysis and interpretation of data (e.g., statistical analysis, biostatistics, computational analysis):** F.M. Jaworski, G. Gueron, R.P. Meiss, E.G. Ortiz, A. Ahmed, N.M. Navone, D.J. Laderach, E.S. Vazquez

**Writing, review, and/or revision of the manuscript:** F.M. Jaworski, L. Gentilini, G. Gueron, P.M. Berguer, A. Ahmed, G.A. Rabinovich, D. Compagno, D.J. Laderach, E.S. Vazquez
**Administrative, technical, or material support (i.e., reporting or organizing data, constructing databases):** G.A. Rabinovich
**Study supervision:** R.P. Meiss, A. Ahmed, D.J. Laderach, E.S. Vazquez

## Acknowledgments

We are grateful to the Prostate Cancer Foundation for the Young Investigator Award 2013 given to G. Gueron, and to the European Molecular Biology Organization for the short-term fellowship awarded to F.M. Jaworski.

## Grant Support

This work was supported by grants ANPCyT PICTRAICES 2013-0996 (to E.S. Vazquez), ANPCyT PICT2012-1533 (to D. Compagno), and ANPCyT PICT2014-0983 (to D.J. Laderach). Argentine National Cancer Institute (to E.S. Vazquez).

The costs of publication of this article were defrayed in part by the payment of page charges. This article must therefore be hereby marked *advertisement* in accordance with 18 U.S.C. Section 1734 solely to indicate this fact.

Received January 12, 2017; revised April 1, 2017; accepted May 10, 2017; published OnlineFirst May 16, 2017.

## References

1. Ferlay J, Soerjomataram I, Ervik M, Dikshit R, Eser S, Mathers C, et al. GLOBOCAN 2012 v1.0, Cancer Incidence and Mortality Worldwide: IARC CancerBase. No. 11 [Internet]. Lyon, France: International Agency for Research on Cancer; 2013.
2. Quail DF, Joyce JA. Microenvironmental regulation of tumor progression and metastasis. Nat Med 2013;19:1423–37.
3. Corn PG. The tumor microenvironment in prostate cancer: elucidating molecular pathways for therapy development. Cancer Manag Res 2012;4: 183–93.
4. Hanna E, Quick J, Libutti SK. The tumour microenvironment: a novel target for cancer therapy. Oral Dis 2009;15:8–17.
5. Grivennikov SI, Greten FR, Karin M. Immunity, inflammation, and cancer. Cell 2010;140:883–99.
6. Mantovani A, Allavena P, Sica A, Balkwill F. Cancer-related inflammation. Nature 2008;454:436–44.
7. Hanahan D, Weinberg RA. Hallmarks of cancer: the next generation. Cell 2011;144:646–74.
8. Jackson JR, Seed MP, Kircher CH, Willoughby DA, Winkler JD. The codependence of angiogenesis and chronic inflammation. FASEB J 1997; 11:457–65.
9. Mantovani A. Molecular pathways linking inflammation and cancer. Curr Mol Med 2010;10:369–73.
10. Gozzelino R, Jeney V, Soares MP. Mechanisms of cell protection by heme oxygenase-1. Annu Rev Pharmacol Toxicol 2010;50:323–54.
11. Wegiel B, Nemeth Z, Correa-Costa M, Bulmer AC, Otterbein LE. Heme oxygenase-1: a metabolic nike. Antioxid Redox Signal 2014;20: 1709–22.
12. Was H, Dulak J, Jozkowicz A. Heme oxygenase-1 in tumor biology and therapy. Curr Drug Targets 2010;11:1551–70.
13. Grochot-Przeczek A, Dulak J, Jozkowicz A. Haem oxygenase-1: non-canonical roles in physiology and pathology. Clin Sci 2012;122:93–103.
14. Gueron G, De Siervi A, Ferrando M, Salierno M, De Luca P, Elguero B, et al. Critical role of endogenous heme oxygenase 1 as a tuner of the invasive potential of prostate cancer cells. Mol Cancer Res 2009;7:1745–55.
15. Ferrando M, Gueron G, Elguero B, Giudice J, Salles A, Leskow FC, et al. Heme oxygenase 1 (HO-1) challenges the angiogenic switch in prostate cancer. Angiogenesis 2011;14:467–79.
16. Ferrando M, Wan X, Meiss R, Yang J, De Siervi A, Navone N, et al. Heme oxygenase-1 (HO-1) expression in prostate cancer cells modulates the oxidative response in bone cells. PLoS One 2013;8:e80315.
17. Gueron G, Giudice J, Valacco P, Paez A, Elguero B, Toscani M, et al. Heme-oxygenase-1 implications in cell morphology and the adhesive behavior of prostate cancer cells. Oncotarget 2014;5:4087–102.
18. Paez A, Pallavicini C, Schuster F, Valacco MP, Giudice J, Ortiz EG, et al. Heme Oxygenase-1 at the forefront of a multi-molecular network that governs cell-cell contact and filopodia-induced zippering in prostate cancer. Cell Death Dis 2016;7:e2570.
19. Elguero B, Gueron G, Giudice J, Toscani MA, De Luca P, Zalazar F, et al. Unveiling the association of STAT3 and HO-1 in prostate cancer: role beyond heme degradation. Neoplasia 2012;14:1043–56.
20. Alaoui-jamali MA, Bismar TA, Gupta A, Szarek WA, Su J, Song W, et al. A novel experimental heme oxygenase-1-targeted therapy for hormone-refractory prostate cancer. Cancer Res 2009;69:8017–24.
21. Li Y, Su J, DingZhang X, Zhang J, Yoshimoto M, Liu S, et al. PTEN deletion and heme oxygenase-1 overexpression cooperate in prostate cancer progression and are associated with adverse clinical outcome. J Pathol 2011; 224:90–100.
22. Wegiel B, Gallo D, Csizmadia E, Harris C, Belcher J, Vercellotti GM, et al. Carbon monoxide expedites metabolic exhaustion to inhibit tumor growth. Cancer Res 2013;73:7009–21.
23. Laderach DJ, Gentilini LD, Giribaldi L, Delgado VC, Nugnes L, Croci DO, et al. A unique galectin signature in human prostate cancer progression suggests galectin-1 as a key target for treatment of advanced disease. Cancer Res 2013;73:86–96.
24. Li ZG, Mathew P, Yang J, Starbuck MW, Zurita AJ, Liu J, et al. Androgen receptor – negative human prostate cancer cells induce osteogenesis in mice through FGF9-mediated mechanisms. J. Clin. Invest 2008;118: 2697–710.
25. Croci DO, Cerliani JP, Dalotto-Moreno T, Méndez-Huergo SP, Mascanfroni ID, Dergan-Dylon S, et al. Glycosylation-dependent lectin-receptor interactions preserve angiogenesis in anti-VEGF refractory tumors. Cell 2014;156:744–58.
26. Rhodes DR, Yu J, Shanker K, Deshpande N, Varambally R, Ghosh D, et al. ONCOMINE: a cancer microarray database and integrated data-mining platform1. Neoplasia 2004;6:1–6.
27. Gentilini LD, Jaworski FM, Tiraboschi C, Gonzalez Perez IG, Kotler ML, Chauchereau A, Laderach D, et al. Stable and high expression of Galectin-8 tightly controls metastatic progression of prostate cancer. Oncotarget 2017 May 18. doi: 10.18632/oncotarget.17963. [Epub ahead of print].
28. Ellerhorst J, Troncoso P, Xu XC, Lee J, Lotan R. Galectin-1 and galectin-3 expression in human prostate tissue and prostate cancer. Urol Res 1999; 27:362–7.
29. Jouve N, Despoix N, Espeli M, Gauthier L, Cypowyj S, Fallague K, et al. The involvement of CD146 and its novel ligand galectin-1 in apoptotic regulation of endothelial cells. J Biol Chem 2013;288:2571–9.
30. Jiang T, Zhuang J, Duan H, Luo Y, Zeng Q, Fan K, et al. CD146 is a coreceptor for VEGFR-2 in tumor angiogenesis. Blood 2012;120:2330–9.
31. Blancou P, Tardif V, Simon T, Rémy S, Carreño L, Kalergis A, et al. Immunoregulatory properties of heme oxygenase-1. Methods Mol Biol 2011;677:431–47.
32. Rabinovich GA, Croci DO. Regulatory circuits mediated by lectin-glycan interactions in autoimmunity and cancer. Immunity 2012;36:322–35.
33. Grasso CS, Wu Y-M, Robinson DR, Cao X, Dhanasekaran SM, Khan AP, et al. The mutational landscape of lethal castration-resistant prostate cancer. Nature 2012;487:239–43.
34. Bouma-Ter Steege JCA, Baeten CIM, Thijssen VLJL, Satijn SA, Verhoeven ICL, Hillen HFP, et al. Angiogenic profile of breast carcinoma determines leukocyte infiltration. Clin Cancer Res 2004;10:7171–8.
35. Vítek L, Gbelcová H, Muchová L, Ván?ová K, Zelenka J, Koníčková R, et al. Antiproliferative effects of carbon monoxide on pancreatic cancer. Dig Liver Dis 2014;46:369–75.
36. Ahmad S, Hewett PW, Fujisawa T, Sissaoui S, Cai M, Gueron G, et al. Carbon monoxide inhibits sprouting angiogenesis and vascular endothelial growth factor receptor-2 phosphorylation. Thromb Haemost 2015;113: 329–37.
37. Croci DO, Salatino M, Rubinstein N, Cerliani JP, Cavallin LE, Leung HJ, et al. Disrupting galectin-1 interactions with N-glycans suppresses

hypoxia-driven angiogenesis and tumorigenesis in Kaposi's sarcoma. J Exp Med 2012;209:1985–2000.
38. Szade A, Grochot-Przeczek A, Florczyk U, Jozkowicz A, Dulak J. Cellular and molecular mechanisms of inflammation-induced angiogenesis. IUBMB Life 2015;67:145–59.
39. Stenzel K, Rubin A, Novogrodsky A. Mitogenic and co-mitogenic properties of hemin. J Immunol 1981;127:2469–73.
40. Graça-Souza AV, Arruda MAB, De Freitas MS, Barja-Fidalgo C, Oliveira PL. Neutrophil activation by heme: implications for inflammatory processes. Blood 2002;99:4160–5.
41. Figueiredo RT, Fernandez PL, Mourao-Sa DS, Porto BN, Dutra FF, Alves LS, et al. Characterization of heme as activator of toll-like receptor 4. J Biol Chem 2007;282:20221–9.
42. Porto BN, Alves LS, Fernández PL, Dutra TP, Figueiredo RT, Graça-Souza AV, et al. Heme induces neutrophil migration and reactive oxygen species generation through signaling pathways characteristic of chemotactic receptors. J Biol Chem 2007;282:24430–6.
43. Schulz S, Chisholm K, Zhao H, Kalish F, Yang Y, Wong R, et al. Heme oxygenase-1 confers protection and alters T-cell populations in a mouse model of neonatal intestinal inflammation. Pediatr Res 2015;77:640–8.
44. Konrad F, Knausberg U, Hone R, Ngamsri K-C, Reutershan J. Tissue heme oxygenase-1 exerts anti-inflammatory effects on LPS-induced pulmonary inflammation. Mucosal Immunol 2016;9:98–111.
45. Nemeth Z, Li M, Csizmadia E, Döme B, Johansson M, Person J, et al. Heme oxygenase-1 in macrophages controls prostate cancer progression. Oncotarget 2015;6:33675–88.
46. Halin Bergstrom S, Halin Bergstrom S, Nilsson M, Adamo H, Thysell E, Jernberg E, et al. Extratumoral heme oxygenase-1 (HO-1) expressing macrophages likely promote primary and metastatic prostate tumor growth. PLoS One 2016;11,e0157280.
47. Jais A, Einwallner E, Sharif O, Gossens K, Lu TTH, Soyal SM, et al. Heme oxygenase-1 drives metaflammation and insulin resistance in mouse and man. Cell 2014;158:25–39.
48. Mashreghi M-F, Klemz R, Knosalla IS, Gerstmayer B, Janssen U, Buelow R, et al. Inhibition of dendritic cell maturation and function is independent of heme oxygenase 1 but requires the activation of STAT3. J Immunol 2008;180:7919–30.
49. Rabinovich GA, Toscano MA. Turning "sweet" on immunity: galectin-glycan interactions in immune tolerance and inflammation. Nat Rev Immunol 2009;9:338–52.